SAINS TANAH – Journal of Soil Science and Agroclimatology

Journal homepage: http://jurnal.uns.ac.id/tanah

Remediation of amoxicillin-contaminated water using zeolite from coal bottom ash

Galuh Yuliani[1], Nedya Tresna Dwi Hidayah[1], Maryono[1], Budiman Anwar[1], Mamun Mollah[2], Jessica Veronica[1], Agus Setiabudi[1]

[1] Chemistry Study Program, Faculty of Mathematics and Natural Sciences Education, Universitas Pendidikan Indonesia, Bandung, 40154, Indonesia
[2] School of Chemistry, Monash University, Clayton Campus, 3800, Australia

ARTICLE INFO

Keywords:
Adsorption
Hydrothermal
Langmuir
ZSM-23

Article history
Submitted: 2024-09-23
Revised: 2025-03-13
Accepted: 2025-06-16
Available online: 2025-08-25
Published regularly: December 2025

***** *Corresponding Author*
Email address:
galuh@upi.edu

ABSTRACT

The contamination of antibiotics in water bodies has increased significantly in recent years. Various treatments, including adsorption, have been sought, but most include expensive sorbent material with low efficiency. This research reported an alternative sorbent material; synthetic zeolite derived from coal-burning waste. Coal bottom ash was converted to zeolite via a hydrothermal technique using various concentrations of NaOH and relatively low-temperature conditions. X-ray diffractogram confirms the formation of ZSM-23 when a 1:2 coal-to-zeolite ratio was used at 95°C. The FTIR spectra also highlighted the characteristics of zeolite functional groups, such as the Si–O vibration at 999.56 cm^{-1} and the Al–O vibration at 799.48 cm^{-1}. The needle-like morphology of ZSM-23 was observed during SEM-EDS analysis. When calculated using BET analysis, the synthetic zeolite also exhibited a high surface area of 433.517 $m^2 g^{-1}$. Upon application in a batch experiment, the maximum adsorption capacity of the zeolite for amoxicillin (AMX) adsorption in aqueous solution was found to be 673.5 mg g^{-1}. The adsorption data fitted the Langmuir isotherm better than the Freundlich one, with a correlation factor of 0.9328. This suggested the monolayer interaction, possibly between the negatively charged zeolite surface and the NH_3^+ group from AMX. However, the physical adsorption mechanism with the zeolite surface may also occur due to the high surface area. Considering the low production cost, this zeolite offers high economic value as an alternative sorbent for removing antibiotics in water effluent.

How to Cite: Yuliani, G., Hidayah, N. T. D., Maryono, Anwar, B., Mollah, M., Veronica, J., & Setiabudi, A. (2025). Remediation of amoxicillin-contaminated water using zeolite from coal bottom ash. Sains Tanah Journal of Soil Science and Agroclimatology, 22(2), 146-154. https://doi.org/10.20961/stjssa.v22i2.93672

1. INTRODUCTION

The penicillin-derived antibiotic amoxicillin (AMX) is one of the most widely used antibiotics for treating various bacterial infections, including those affecting the gastrointestinal, respiratory, and skin systems (Ali & Maafa, 2024). According to the World Health Organisation (WHO), this antibiotic is of utmost importance as an antimicrobial medicine, leading to its high consumption and utilisation (Batista et al., 2020). Although AMX is essential for treatment, its widespread use has led to it becoming one of the most commonly found contaminants in the environment. The use of antibiotics in high-income countries has decreased in recent years due to compliance with health organisations' regulatory strategies. However, antibiotic consumption in low and middle-income countries is still very high. In Indonesia, around 75% of patients hospitalised had been given antibiotics, even without any bacterial coinfection symptoms (Yossadania et al., 2023). High consumption of antibiotics poses a significant risk of water contamination. Antibiotic concentration in one water effluent treatment facility before the COVID-19 pandemic was reported to be 1.6 µg L^{-1}, but after the pandemic, it was reported to be 509.64 µg L^{-1} (Samandari et al., 2022).

Like other antibiotics, amoxicillin, when administered to humans and animals, is excreted in feces and urine without degradation (Zhang et al., 2019). Animal feces are commonly used as a nutrient-rich fertilizer, leading to direct contamination of the environment. Feces and urine may also enter the body of water and bioaccumulate in fish, thus entering the human food chain. This will significantly increase the availability of antibiotic resistance elements, which may

STJSSA, p-ISSN 1412-3606 e-ISSN 2356-1424
http://dx.doi.org/10.20961/stjssa.v22i2.93672

have severe consequences for both human and animal health (Larsson & Flach, 2022). The residual antibiotics have been labeled as emerging contaminants of concern, and various water treatment methods must be explored to address this issue. Bhargava et al. (2018) have explored conventional water treatment methods, such as advanced oxidation, hydrolysis, and photodegradation. However, these methods were considered impractical and may result in secondary by-products requiring further treatments. Jiang et al. (2018) and Renu et al. (2017) mentioned that adsorption may be a practical and preparative alternative. Furthermore, sorbent materials used in this method must have high adsorption capacity, be cheap, and be readily available. Among various sorbent materials, zeolite stands out for its high porosity and sorption capacity, and is applicable over a wide range of temperatures (Luo et al., 2021). Zeolite has been utilized in separation, filtration, ion exchange processes, catalysis, and adsorption due to its extensive internal pores and negatively charged surface (Jiang et al., 2020). Unfortunately, synthetic zeolite is expensive when prepared using pure chemical precursors. Thus, alternative starting materials are sought. Some potential starting materials include coal ash, red mud, and kaolin (Yadav et al., 2021). Due to the creation of numerous disposal problems, waste materials, such as coal ash, are arguably the most promising starting material for zeolite (Jiang et al., 2018)). Coal ash utilisation may become an alternative solution for coal waste recycling, potentially reducing the environmental effects of coal processing in many countries (Luo et al., 2021).

Coal ash contains silica (SiO_2) and alumina (Al_2O_3) as main components; additionally, it also contains iron oxides (Fe_2O_3), carbon, magnesium, sulfur, and trace elements. The high percentages of SiO_2 and Al_2O_3 in the ash composition enable coal ash utilisation as starting materials for zeolite synthesis (Liu, 2022). Although coal ash zeolite synthesis has been reported in numerous studies, variations in synthesis methods and types of zeolite produced persist. Some types of zeolite that are commonly reported include Na-X, Na-P1, zeolite X, zeolite A, and SSZ-13 zeolite (Boycheva et al., 2021; Gollakota et al., 2021; Nowak et al., 2021; Tumrani et al., 2021). One type of zeolite rarely reported is the ZSM type. This type is exciting due to its unique structure and high porosity, such as ZSM-23 with a specific surface area of 880.05 $m^2 g^{-1}$ (Lin & Chen, 2021). The sorption capacity of this zeolite for iodine and heavy metals was higher than that of commercial activated carbon. Aside from the sorption capacity values, an adsorption study is important in categorising the adsorption mechanism based on various adsorption isotherms. Such a study will help to gain a deeper understanding of the interaction between sorbent materials and sorbed molecules.

Therefore, this research aims to convert coal bottom ash into ZSM-type zeolite and use it to remediate amoxicillin-contaminated water. An adsorption study was also conducted to understand the adsorption mechanism. Based on this adsorption study, the interaction between ZSM-type zeolite as sorbent materials and AMX as sorbed species may be proposed.

2. MATERIAL AND METHODS

2.1. Material

Coal bottom ash (CBA) was obtained from a local food industry in West Java, Indonesia, using sub-bituminous coal as fuel. Amoxicillin (AMX), sodium hydroxide, aquadest, and hydrochloric acid were purchased from Merck. The experiment was conducted in the Materials Research Laboratory of the Chemistry Study Program at UPI, Bandung.

2.2. Methods

The zeolite synthesis methods adopted the hydrothermal technique previously reported in the literature (Tumrani et al., 2021). Ten grams of CBA was mixed with NaOH in ratios of 1:1, 1:1.5, and 1:2, and was placed in a Teflon autoclave at different temperatures (65, 80, and 95°C) for 9 hours. The solid product was washed with deionized water (Aquadest) until a pH of 7 was reached, dried at 110°C for 9 hours, and sieved using a 100-mesh sieve. The zeolite powder was analysed using *Scanning Electron Microscopy-Energy Dispersive Spectrometry* (SEM-EDS), *X-ray Diffraction* (XRD), *Fourier Transformed Infrared* (FTIR), and *Brunauer*, *Emmett*, and *Teller* (BET) surface analysis.

In the adsorption study, 0.05 g of zeolite was mixed with 25 mL of AMX solutions having different concentrations (2, 4, 5, & 6 ppm). The mixture was fixed to a pH of 5 and was shaken for 90 minutes at 200 rpm. The supernatant was centrifuged at 3000 rpm for 10 minutes. The residual concentrations of AMX were analyzed using a Shimadzu LC-MS/MS system (model 8045). The mobile phase consisted of a 20% ammonium acetic buffer solution and 1% v/v formic acid in water (80%). The sample volume injected was 1 µL for 5 minutes, and the m/z selected were 366.05 > 114.00 and 366.05 > 349.00. The data were collected based on one measurement; no statistical tools were used. The residual concentration data were collected as C_e (mg L^{-1}), and the adsorbed amount, Q_e (mg g^{-1}), was calculated according to Equation 1 (Chwastowski et al., 2023).

$$Q_e = \frac{(C_o - C_e) \times V}{M} \quad \text{.....[1]}$$

Where C_e is the equilibrium concentration of AMX, C_o is the initial concentration, V is the total volume of the solution, and M is the weight of the zeolite. The adsorption isotherms were analyzed using the two most common models, Langmuir and Freundlich. Equation 2 provides the Langmuir equation.

$$\frac{C_e}{Q_e} = \frac{1}{b \times Q_m} + \frac{C_e}{Q_m} \quad \text{.....[2]}$$

Where b is the Langmuir constant, and Q_m is the maximum adsorption capacity.

The linear plot of $\frac{C_e}{Q_e}$ vs C_e was analysed to obtain Q_m. Additionally, the coefficient of determination, R-squared (R^2), derived from the linear regression, provides information about the alignment of the adsorption data with the Langmuir model. The Freundlich equation is provided in Equation 3.

$$\log Q_e = \log K + \frac{1}{n} \log C_e \quad \text{.....[3]}$$

Where n and K are Freunclich constants. The linear plot of $\log Q_e$ vs log K was analyzed, and the coefficient of determination, R-squared (R^2), was evaluated. This calculation was conducted using Microsoft Excel® with regression analysis.

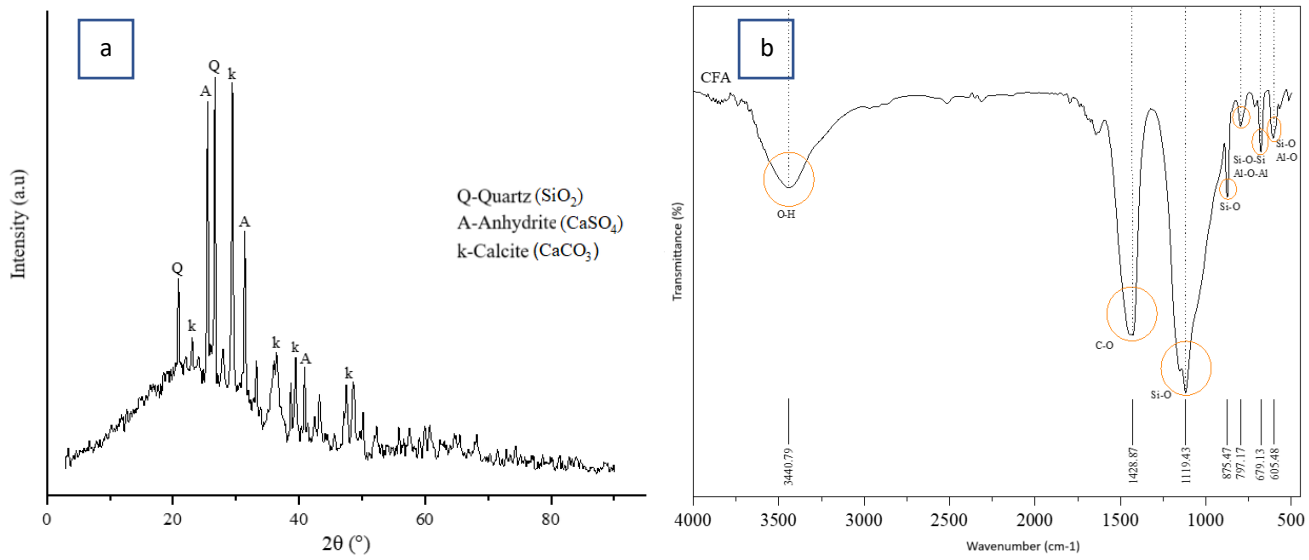

Figure 1. CBA analyses: **(a)** XRD pattern and **(b)** FTIR spectrum

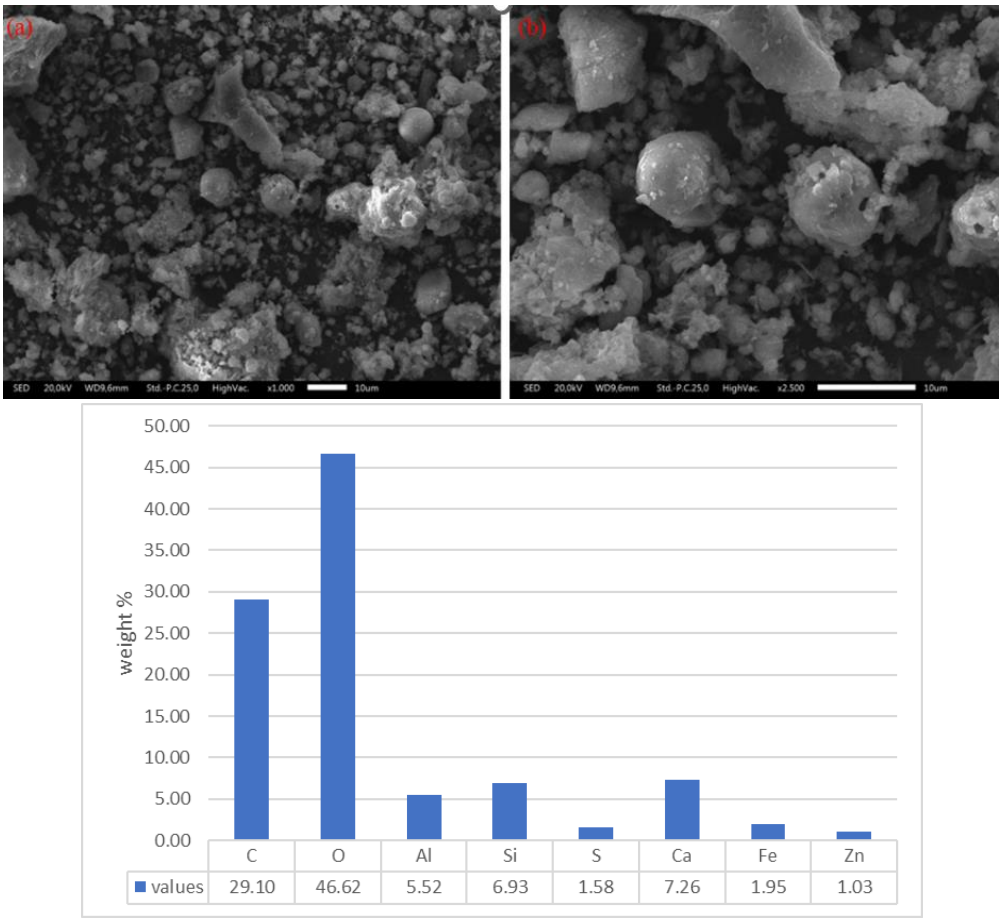

Figure 2. SEM photos at magnification of: (a) 1000×, (b) 2500×, and (c) EDS composition analysis

3. RESULTS

3.1. Coal bottom ash (CBA) analyses

The crystal phases detected from CBA are shown in Figure 1a, which include quartz (SiO_2), calcium sulfate ($CaSO_4$), and calcite ($CaCO_3$) as the dominant peaks. FTIR analysis in Figure 1b was conducted to characterise the functional groups that predominated in the CBA structure. XRD analysis confirmed characteristic peaks for quartz at 1119.45 and 875.47 cm^{-1} for Si-O asymmetric vibration, at 605.48 cm^{-1} for Si-O and Al-O vibrations, 797.17 and 679.13 cm^{-1} for Si–O–Si and Al–O–Al. The characteristic peak for calcite was found at 1428.87 cm^{-1} for C–O. Other detected functional groups included hydroxyls at 3440.79 cm^{-1}, corresponding to the O–H vibration (Makgabutlane et al., 2020; Mokgehle et al., 2020; Zainal Abidin et al., 2017).

The surface morphology and elemental analysis of the CBA sample were studied using SEM-EDS, as shown in Figure 2. SEM photos showed that the CBA particles were

mostly spherical with an average diameter of 20 µm, which represents amorphous aluminium silica (Argiz et al., 2017). In line with XRD and FTIR analyses, EDS results confirmed the presence of Al, Si, Ca, C, and O in the CBA structure. A small percentage of Fe (magnetite) was also found, at less than 4%.

3.2. Zeolite analyses

X-ray diffraction is used as one basic yet powerful tool for zeolite characterisation. This analysis is instrumental in confirming the phase compositions and structures of zeolites and related microporous materials. The XRD analysis results for zeolite synthesised with a CBA to NaOH ratio of 1:2 at varying temperatures of 65°C, 80°C, and 95°C highlight the significant influence of temperature on zeolite phase formation (Fig. 3a). The sodium silicate hydrate peaks appeared at 2θ values of 20.89°, 26.65°, 29.33°, and 31.34° at 65°C. A similar trend was observed at 80°C, with zeolite peaks at 2θ values of 18.95°, 26.65°, 29.08°, and 31.33°. These patterns indicate the formation of ZSM-23 zeolites (marked by z). However, phase X was observed at 2θ values of 24.19° and 24.26° in both 65°C and 80°C, as per JCPDS card no. 28–1036, indicating incomplete conversion. A pattern was observed at 95°C, with more distinct and sharper zeolite peaks, confirming the complete formation of ZSM-23 (Zeolite Socony Mobil-23) as per the JCPDS card number 43-0582. Additionally, no phase X was observed in the 95°C XRD pattern, indicating a higher purity of ZSM-23. The XRD pattern of ZSM-23 was observed at 2θ values of 13.90°, 19.02°, 20.81°, 24.22°, 26.58°, 31.26°, 35.49°, and 42.64°.

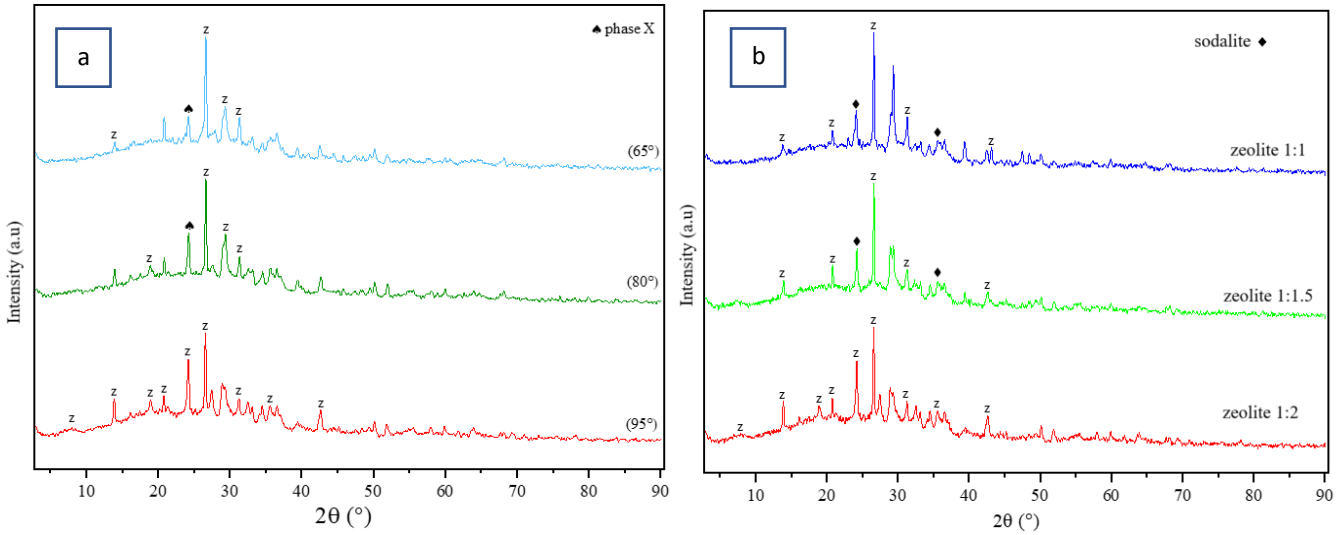

Figure 3. Diffractograms of zeolite product at (a) CBA to NaOH ratio of 1:2 and different temperatures, (b) 95°C and different CBA to NaOH ratios

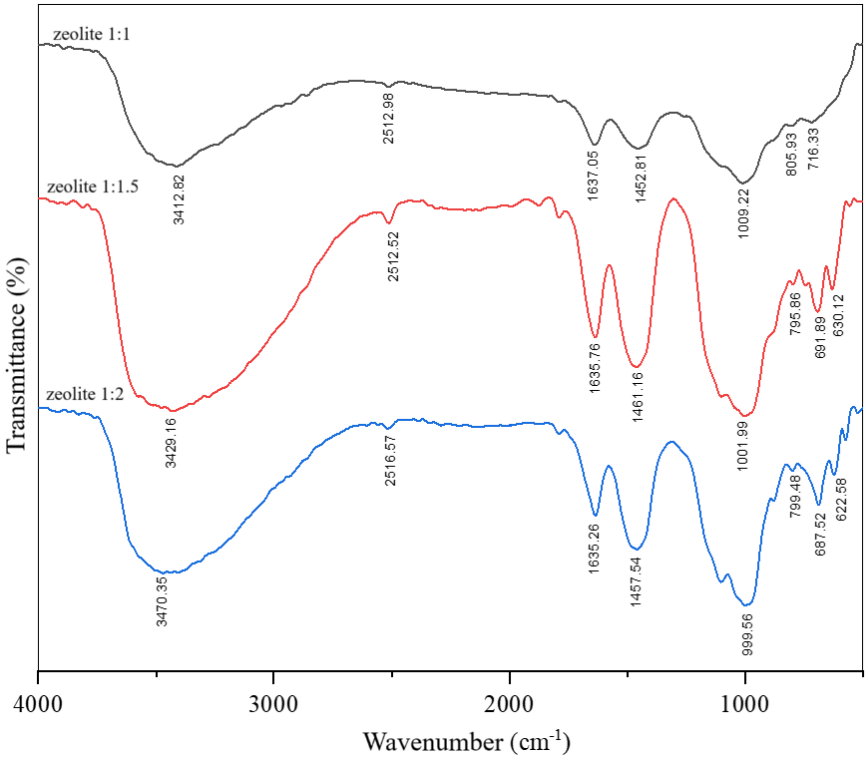

Figure 4. FTIR spectra of various zeolite samples

The effect of CBA to NaOH ratios on zeolite formation was also studied by conducting 1:1, 1:1.5, and 1:2 reactions at 95°C (Fig. 3b). Similar peak patterns were observed for CBA to NaOH ratios of 1:1 and 1:1.5, with zeolite peaks detected at 2θ values of 13.8°, 20.8°, 26.6°, 31.3°, and 43.0 °. However, sodalite peaks also appeared in both products according to the JCPDS card no. 43-0141 (Arnelli et al., 2018). The formation of ZSM-23, a more desired product, was confirmed when the CBA to NaOH ratio was 1:2, a favourable ratio due to its higher surface area and better crystallinity (ACS Material, n.d.).

FTIR analysis (Fig. 4) showed that the hydroxyls (O−H) vibration was observed in all zeolite samples at around 3400 cm^{-1}. Characteristic vibrations for Si−O or Al−O at 1400 cm^{-1} and 1000 cm^{-1} were observed for all zeolite samples. Double-ring structures of zeolite compounds resulted in vibrations at around 620-630 cm^{-1}, with peak sharpness signifying strong zeolite characteristics. Additional vibrations associated with O–H bonding from water molecules were detected at 2930-3650 cm^{-1}, 2500 cm^{-1}, 1630 cm^{-1}, and 650-950 cm^{-1} (Almeida et al., 2025).

SEM analysis confirmed the surface morphology of the zeolite product (Chen et al., 2020), with photos at magnifications of 10,000× and 20,000× shown in Figure 5. It was clear that the zeolite had the typical needle-shaped morphology. Zeolite resulting from a CBA to NaOH ratio of 1:1 exhibits a subtle needle-like morphology. However, as the NaOH ratio increases, the zeolite products show more distinct needle-like morphology, as evident upon 20,000x magnification.

The BET analysis was conducted to measure the surface area and porosity of the zeolite samples, as shown in Table 1. The zeolite with a CBA to NaOH ratio of 1:2 exhibits the highest surface area of 433 $m^2\ g^{-1}$ and a pore volume of 1.18 $cm^3\ g^{-1}$. Other zeolite products have surface areas of less than 60 $m^2\ g^{-1}$, which is lower than that of the raw bottom ash.

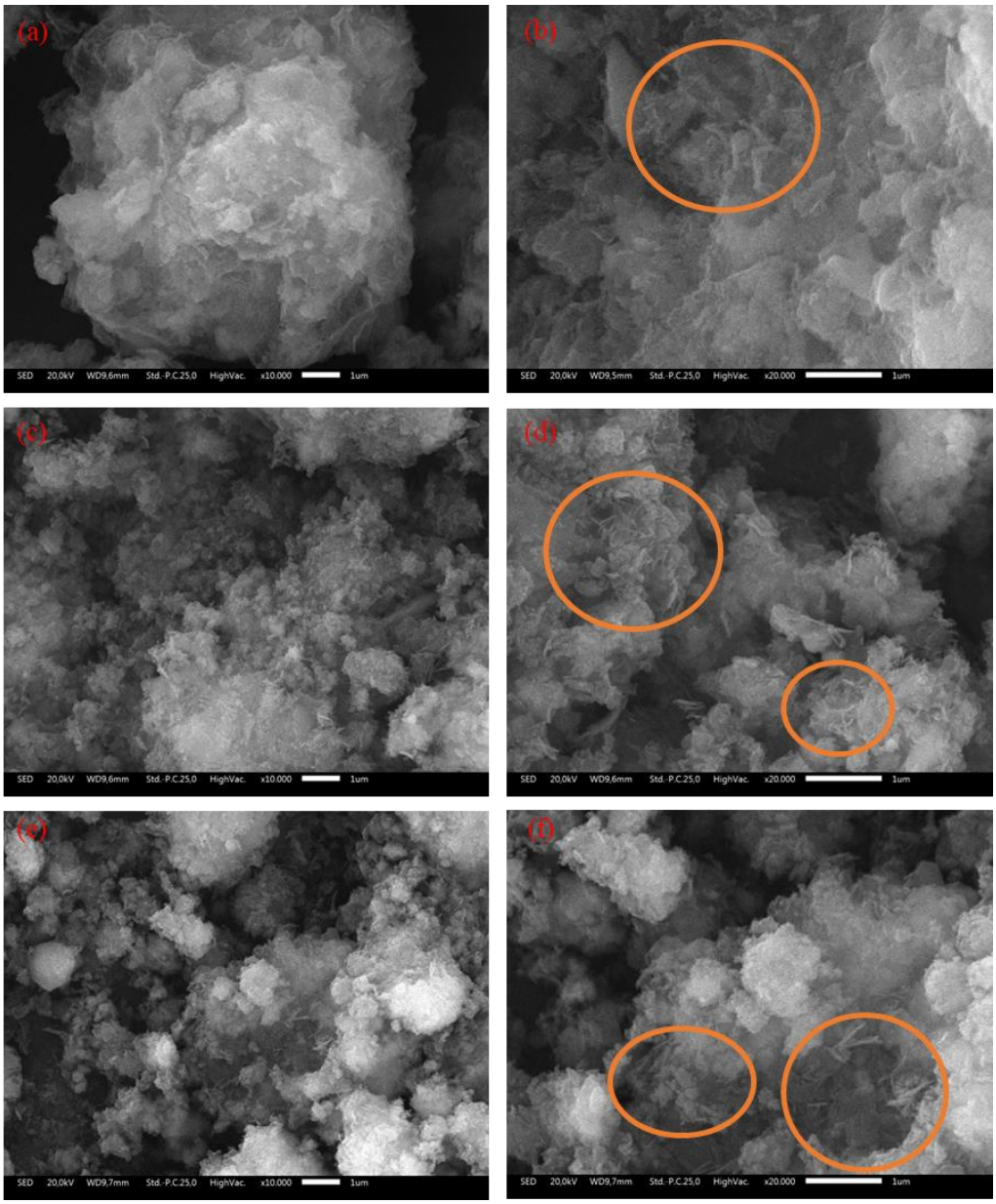

Figure 5. SEM photos of zeolite products with CBA to NaOH of (a) 1:1 at a magnification of 10,000× (b) 1:1 at a magnification of 20,000×, (c) 1:1.5 at a magnification of 10,000× (d) 1:1.5 at a magnification of 20,000×, (d) 1:2 at a magnification of 10,000× (f) 1:2 at a magnification of 20,000×

Table 1. Surface area, pore volume, and pore diameter of zeolite samples

Sample name	Surface area (m^2/g)	Pore volume (cm^3/g)	Pore diameter (nm)
CBA	208.876	0.2714	157.29
Zeolite with a CBA to NaOH ratio of 1:1	59.128	0.6316	158.21
Zeolite with a CBA to NaOH ratio of 1:1.5	48.837	0.5864	221.76
Zeolite with a CBA to NaOH ratio of 1:2	433.517	1.1810	178.98

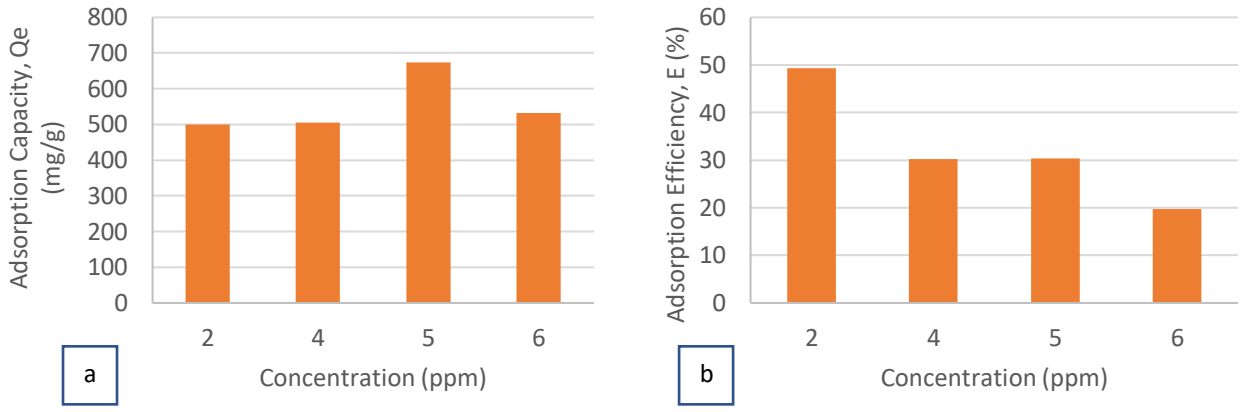

Figure 6. (a) The adsorption capacity of zeolite with a CBA to NaOH ratio of 1:2 for AMX and (b) its adsorption efficiency

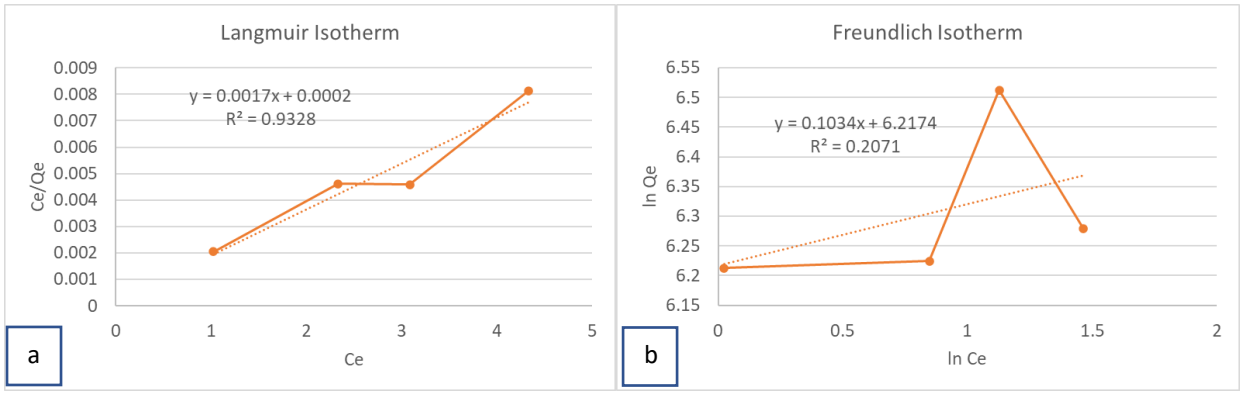

Figure 7. Adsorption isotherm plots: (a) Langmuir and (b) Freundlich

3.3. Adsorption study

Based on the confirmation of ZSM-23 formation derived from XRD and SEM analyses, the adsorption study was only conducted on the zeolite with a CBA to NaOH ratio of 1:2. Adsorption data are presented in Figure 6. The adsorption capacity of the zeolite was measured to be above 670 mg g^{-1} at an AMX concentration of 5 ppm.

Two adsorption isotherm models, the Langmuir and the Freundlich models, were used to analyze the adsorption data (Fig. 7). The data were plotted using Langmuir and Freundlich isotherms, and the conformity of the data with these isotherms was compared. The data plots fitted the Langmuir isotherm model better than the Freundlich model, with a correlation factor (R^2) value of 0.9328. On the other hand, the Freundlich plot shows poor alignment with a correlation factor value of 0.2071.

4. DISCUSSION

Based on the results of the XRD and FTIR analysis (Fig. 1), the peak composition obtained confirms the typical CBA as reported in the literature (Kalinkin et al., 2020). Minerals such as quartz, calcite, mullite, hematite, and portlandite are commonly found in the mineral composition of biomass ashes, although their amounts may vary across different samples. SEM-EDS photo showing a small presence of Fe is desirable for zeolite synthesis because it can inhibit zeolite formation (Fig. 2). During the conversion of SiO_2 and Al_2O_3 to zeolite, magnetite can act as a contaminant, leading to the formation of other mineral phases, such as sodalite (Su et al., 2023).

Zeolite synthesis using the hydrothermal method was selected due to the lower operational temperature and the high crystallinity of the resulting product. Factors affecting the hydrothermal reaction include temperature and sodium hydroxide composition in the reaction mixture (Asgar Pour et al., 2023). Based on the XRD analyses (Fig. 3a), it is known that the higher the operating temperature, the greater the collision frequency and reaction rate, resulting in a more crystalline zeolite phase in the diffractogram. This confirms that the nucleation mechanism and crystal growth in the crystallisation process are affected by temperature (Asgar Pour et al., 2023). Additionally, NaOH acts as an activator in

forming silicate aluminates in the aqueous solution during zeolite formation. Hence, higher NaOH concentration may facilitate better conversion (Fig. 3b). Meanwhile, based on the results of the FTIR analysis shown in Figure 4, a wider O–H peak was detected in the zeolite product compared to that of the CBA, due to the formation of more hydrogen bonds from the sodium salt attached to the zeolite (Schroeder et al., 2022). Moreover, incorporating sodium into the zeolite structure increases its hygroscopicity compared to CBA (Touloumet et al., 2023). The XRD analyses confirmed the presence of the zeolite phase resulting from CBA conversion. The 2θ values were extracted from the diffractogram data and compared to the JCPDS card number 43-0141, confirming the ZSM-23 type. Additionally, the SEM analysis also shows a needle-like morphology (Fig. 5), common to ZSM-23-type zeolites (Chen et al., 2020; Chen et al., 2017; Uvarkina et al., 2015). This needle-like shape was more evident at the CBA to NaOH ratio of 1:2, indicating a more complete conversion.

Several factors that influence the performance of zeolite as a sorbent material are surface area and porosity. Based on the BET results, the zeolite with a CBA to NaOH ratio of 1:2 has the highest surface area and pore volume, with the values of 433 $m^2 g^{-1}$ and 1.18 $cm^3 g^{-1}$, respectively (Table 1). Zeolite samples with CBA to NaOH ratios of 1:1 and 1:1.5 showed very low porosity and surface areas, suggesting partial conversion and incomplete pore formation. This suggests that the zeolite with a CBA to NaOH ratio of 1:2 may perform better than other sorbent samples and was chosen for the adsorption study.

The adsorption study was conducted using only the zeolite with a CBA to NaOH ratio of 1:2 as sorbent materials for a model amoxicillin (AMX) solution at pH 5, based on the literature (Jafari et al., 2018). Residual AMX concentrations were determined using LC-MS/MS, a highly sensitive instrument for antibiotic concentration measurement in aqueous solution (Radovanovic et al., 2022). Based on the adsorption data obtained, the adsorption efficiency decreased at higher AMX concentrations (Fig. 6), possibly due to the saturation of the zeolite surface (Balarak et al., 2017).

The adsorption mechanism was studied by plotting the adsorption data using the Langmuir and the Freundlich isotherm models. Isothermal modelling indicates a better fit with the Langmuir isotherm model, which assumes monolayer adsorption of adsorbate molecules on the sorbent surface (Butyrskaya, 2024), primarily driven by electrostatic interactions (Kecili & Hussain, 2018). The zeolite surface is negatively charged, and the AMX molecule has $-NH^{3+}$ anionic species; these opposite charges attract each other, resulting in an electrostatic interaction. This possible interaction is depicted in Figure 8. The electrostatic interaction that occurred may lead to the adsorption of AMX onto the zeolite surface via a chemical interaction (or chemisorption). However, due to the high surface area of ZSM-23 zeolite, the physisorption (via available pores) may also play a significant role (Travkina et al., 2024). Therefore, it can be concluded that both chemisorption and physisorption play important roles in the adsorption mechanism of AMX onto ZSM-23 (Ray et al., 2020).

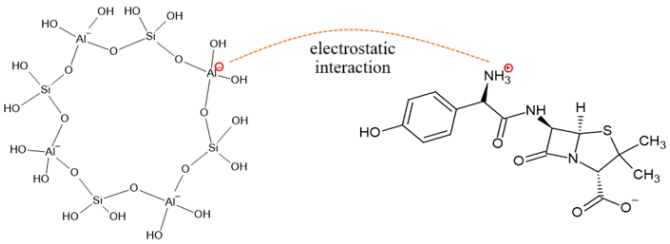

Figure 8. Proposed interactions between AMX and ZSM-23

The adsorption data were analyzed based on a single measurement; this approach could be improved by adding more replication and varying the concentration values. The zeolite synthesis may also benefit from increasing the temperature to above 100 °C to determine if the ZSM-type remains prevalent or if other zeolite phases have arisen. The adsorption mechanism study may also be improved by adding other isotherm models to see how the data fits, such as the Temkin, Sips, or Redlich-Peterson models.

5. CONCLUSION

The coal bottom ash (CBA) has been successfully converted to a ZSM-23 type zeolite at a CBA-to-NaOH ratio of 1:2 and 95°C. The zeolite was confirmed to have a needle-like morphology and a high surface area of 433.517 $m^2 g^{-1}$. Upon its utilisation as a sorbent material for amoxicillin (AMX) adsorption, the maximum adsorption capacity was 673.5 m g^{-1}. The adsorption data were plotted using adsorption isotherm models, and the result indicated alignment with the Langmuir isotherm model. The adsorption mechanism was assumed to form a monolayer adsorption, probably via electrostatic interaction. However, considering the high surface area of the zeolite, physisorption may also predominate as an alternative mechanism.

Declaration of Competing Interest

The authors declare that no competing financial or personal interests may appear to influence the work reported in this paper.

References

ACS Material. (n.d.). *Technical Data Sheet: ACS Material ZSM-23*. Retrieved August 15, 2022 from https://www.acsmaterial.com/zsm-23.html

Ali, M. A., & Maafa, I. M. (2024). Photodegradation of Amoxicillin in Aqueous Systems: A Review. *International Journal of Molecular Sciences*, *25*(17), 9575. https://doi.org/10.3390/ijms25179575.

Almeida, J. N., Song, L., Askarli, S., Chung, S.-H., & Ruiz-Martínez, J. (2025). Zeolite–Water Chemistry: Characterization Methods to Unveil Zeolite Structure. *Chemistry–Methods*, *5*(4), e202400076. https://doi.org/10.1002/cmtd.202400076.

Argiz, C., Sanjuán, M. Á., & Menéndez, E. (2017). Coal Bottom Ash for Portland Cement Production. *Advances in Materials Science and Engineering*, *2017*(1), 6068286. https://doi.org/10.1155/2017/6068286.

Arnelli, A., Fathoni, B. Y., Prastyo, T. I., Suseno, A., & Astuti, Y. (2018). Synthesis of Zeolite from Bagasse and Rice

Husk Ashes as Surfactant Builder on Detergency Process: Variation of NaOH Concentration for Silica Isolation [zeolite, surfactant builder, detergency, rice husk, ash bagasse]. *2018*, *21*(3), 5. https://doi.org/10.14710/jksa.21.3.139-143.

Asgar Pour, Z., Alassmy, Y. A., & Sebakhy, K. O. (2023). A Survey on Zeolite Synthesis and the Crystallization Process: Mechanism of Nucleation and Growth Steps. *Crystals*, *13*(6), 959. https://doi.org/10.3390/cryst13060959.

Balarak, D., Mostafapour, F. K., Akbari, H., & Joghtaei, A. (2017). Adsorption of Amoxicillin Antibiotic from Pharmaceutical Wastewater by Activated Carbon Prepared from Azolla filiculoides. *Journal of Pharmaceutical Research International*, *18*(3), 1-13. https://doi.org/10.9734/JPRI/2017/35607.

Batista, A. D., A. Rodrigues, D., Figueiras, A., Zapata-Cachafeiro, M., Roque, F., & Herdeiro, M. T. (2020). Antibiotic Dispensation without a Prescription Worldwide: A Systematic Review. *Antibiotics*, *9*(11), 786. https://doi.org/10.3390/antibiotics9110786.

Bhargava, A., Arivu, P., Chandera, N., & Govani, J. (2018). An overview of waste management in Indian perspective. *Global Journal of Energy and Environment*, *6*(3), 158-161.

Boycheva, S., Zgureva, D., Lazarova, H., & Popova, M. (2021). Comparative studies of carbon capture onto coal fly ash zeolites Na-X and Na–Ca-X. *Chemosphere*, *271*, 129505. https://doi.org/10.1016/j.chemosphere.2020.129505.

Butyrskaya, E. (2024). Understanding the mechanism of monolayer adsorption from isotherm. *Adsorption*, *30*(6), 1395-1406. https://doi.org/10.1007/s10450-024-00512-4.

Chen, X., Xi, H., Chen, C., Ma, Z., & Hou, B. (2020). Synthesis of ZSM-23 Zeolite by Two-Stage Temperature-Varied Crystallization and Its Isomerization Performance. *Applied Sciences*, *10*(21), 7546. https://doi.org/10.3390/app10217546.

Chen, Y., Li, C., Wang, L., Zhang, M., & Liang, C. (2017). Seed-assisted synthesis of ZSM-23 zeolites in the absence of alkali metal ions. *Microporous and Mesoporous Materials*, *252*, 146-153. https://doi.org/10.1016/j.micromeso.2017.06.013.

Chwastowski, J., Guzik, M., Bednarz, S., & Staroń, P. (2023). Upcycling Waste Streams from a Biorefinery Process—A Case Study on Cadmium and Lead Biosorption by Two Types of Biopolymer Post-Extraction Biomass. *Molecules*, *28*(17), 6345. https://doi.org/10.3390/molecules28176345.

Gollakota, A. R. K., Munagapati, V. S., Volli, V., Gautam, S., Wen, J.-C., & Shu, C.-M. (2021). Coal bottom ash derived zeolite (SSZ-13) for the sorption of synthetic anion Alizarin Red S (ARS) dye. *Journal of Hazardous Materials*, *416*, 125925. https://doi.org/10.1016/j.jhazmat.2021.125925.

Jafari, K., Heidari, M., & Rahmanian, O. (2018). Wastewater treatment for Amoxicillin removal using magnetic adsorbent synthesized by ultrasound process. *Ultrasonics Sonochemistry*, *45*, 248-256. https://doi.org/10.1016/j.ultsonch.2018.03.018.

Jiang, N., Erdős, M., Moultos, O. A., Shang, R., Vlugt, T. J. H., Heijman, S. G. J., & Rietveld, L. C. (2020). The adsorption mechanisms of organic micropollutants on high-silica zeolites causing S-shaped adsorption isotherms: An experimental and Monte Carlo simulation study. *Chemical Engineering Journal*, *389*, 123968. https://doi.org/10.1016/j.cej.2019.123968.

Jiang, N., Shang, R., Heijman, S. G. J., & Rietveld, L. C. (2018). High-silica zeolites for adsorption of organic micro-pollutants in water treatment: A review. *Water Research*, *144*, 145-161. https://doi.org/10.1016/j.watres.2018.07.017.

Kalinkin, A. M., Gurevich, B. I., Myshenkov, M. S., Chislov, M. V., Kalinkina, E. V., Zvereva, I. A., . . . Petkova, V. (2020). Synthesis of Fly Ash-Based Geopolymers: Effect of Calcite Addition and Mechanical Activation. *Minerals*, *10*(9), 827. https://doi.org/10.3390/min10090827.

Kecili, R., & Hussain, C. M. (2018). Chapter 4 - Mechanism of Adsorption on Nanomaterials. In C. M. Hussain (Ed.), *Nanomaterials in Chromatography* (pp. 89-115). Elsevier. https://doi.org/10.1016/B978-0-12-812792-6.00004-2

Larsson, D. G. J., & Flach, C.-F. (2022). Antibiotic resistance in the environment. *Nature Reviews Microbiology*, *20*(5), 257-269. https://doi.org/10.1038/s41579-021-00649-x.

Lin, Y.-J., & Chen, J.-C. (2021). Resourcization and valorization of waste incineration fly ash for the synthesis of zeolite and applications. *Journal of Environmental Chemical Engineering*, *9*(6), 106549. https://doi.org/10.1016/j.jece.2021.106549.

Liu, H. (2022). Conversion of Harmful Fly Ash Residue to Zeolites: Innovative Processes Focusing on Maximum Activation, Extraction, and Utilization of Aluminosilicate. *ACS Omega*, *7*(23), 20347-20356. https://doi.org/10.1021/acsomega.2c02388.

Luo, Y., Wu, Y., Ma, S., Zheng, S., Zhang, Y., & Chu, P. K. (2021). Utilization of coal fly ash in China: a mini-review on challenges and future directions. *Environmental Science and Pollution Research*, *28*(15), 18727-18740. https://doi.org/10.1007/s11356-020-08864-4.

Makgabutlane, B., Nthunya, L. N., Nxumalo, E. N., Musyoka, N. M., & Mhlanga, S. D. (2020). Microwave Irradiation-Assisted Synthesis of Zeolites from Coal Fly Ash: An Optimization Study for a Sustainable and Efficient Production Process. *ACS Omega*, *5*(39), 25000-25008. https://doi.org/10.1021/acsomega.0c00931.

Mokgehle, T. M., Gitari, W. M., & Tavengwa, N. T. (2020). Synthesis and characterization of zeolites produced by ultrasonication of coal fly Ash/NaOH slurry filtrates. *South African Journal of Chemistry*, *73*(1), 64–69-64–69. https://doi.org/10.17159/0379-4350/2020/v73a10

Nowak, P., Muir, B., Solińska, A., Franus, M., & Bajda, T. (2021). Synthesis and Characterization of Zeolites Produced from Low-Quality Coal Fly Ash and Wet Flue

Gas Desulphurization Wastewater. *Materials*, *14*(6), 1558. https://doi.org/10.3390/ma14061558.

Radovanovic, M., Day, R. O., Jones, G. D. R., Galettis, P., & Norris, R. L. G. (2022). LC–MS/MS method for simultaneous quantification of ten antibiotics in human plasma for routine therapeutic drug monitoring. *Journal of Mass Spectrometry and Advances in the Clinical Lab*, *26*, 48-59. https://doi.org/10.1016/j.jmsacl.2022.11.001.

Ray, S. S., Gusain, R., & Kumar, N. (2020). Chapter four - Adsorption in the context of water purification. In S. S. Ray, R. Gusain, & N. Kumar (Eds.), *Carbon Nanomaterial-Based Adsorbents for Water Purification* (pp. 67-100). Elsevier. https://doi.org/10.1016/B978-0-12-821959-1.00004-0

Renu, Agarwal, M., & Singh, K. (2017). Methodologies for removal of heavy metal ions from wastewater: an overview. *Interdisciplinary Environmental Review*, *18*(2), 124-142. https://doi.org/10.1504/IER.2017.087915.

Samandari, M., Movahedian Attar, H., Ebrahimpour, K., & Mohammadi, F. (2022). Monitoring of Amoxicillin and Cephalexin Antibiotics in Municipal WWTPs During Covid-19 Outbreak: A Case Study in Isfahan, Iran. *Air, Soil and Water Research*, *15*, 11786221221103879. https://doi.org/10.1177/11786221221103879.

Schroeder, C., Zones, S. I., Hansen, M. R., & Koller, H. (2022). Hydrogen Bonds Dominate Brønsted Acid Sites in Zeolite SSZ-42: A Classification of Their Diversity. *Angewandte Chemie International Edition*, *61*(3), e202109313. https://doi.org/10.1002/anie.202109313.

Su, Q., Wei, X., Yang, G., Ou, Z., Zhou, Z., Huang, R., & Shi, C. (2023). In-situ conversion of geopolymer into novel floral magnetic sodalite microspheres for efficient removal of Cd(II) from water. *Journal of Hazardous Materials*, *453*, 131363. https://doi.org/10.1016/j.jhazmat.2023.131363.

Touloumet, Q., Postole, G., Massin, L., Lorentz, C., & Auroux, A. (2023). Investigation of the impact of zeolite shaping and salt deposition on the characteristics and performance of composite thermochemical heat storage systems [10.1039/D2TA07615B]. *Journal of Materials Chemistry A*, *11*(6), 2737-2753. https://doi.org/10.1039/D2TA07615B.

Travkina, O. S., Serebrennikov, D. V., Kuvatova, R. Z., Khazipova, A. N., Filippova, N. A., Agliullin, M. R., & Kutepov, B. I. (2024). The Synthesis of Granular ZSM-23 Zeolite with a High Degree of Crystallinity and a Micro-Meso-Macroporous Structure, and Its Use in the Hydroisomerization of n-Hexadecane. *Nanomaterials*, *14*(23), 1897. https://doi.org/10.3390/nano14231897.

Tumrani, S. H., Soomro, R. A., Zhang, X., Bhutto, D. A., Bux, N., & Ji, X. (2021). Coal fly ash driven zeolites for the adsorptive removal of the ceftazidime drug [10.1039/D1RA02785A]. *RSC Advances*, *11*(42), 26110-26119. https://doi.org/10.1039/D1RA02785A.

Uvarkina, D. D., Piryutko, L. V., Danilova, I. G., Budukva, S. V., Klimov, O. V., Kharitonov, A. S., & Noskov, A. S. (2015). Effect of boron on acid and catalytic properties of Pd-ZSM-23/Al2O3 catalysts in the reaction of diesel fuel hydroisomerization. *Russian Journal of Applied Chemistry*, *88*(11), 1827-1838. https://doi.org/10.1134/S10704272150110142.

Yadav, V. K., Choudhary, N., Tirth, V., Kalasariya, H., Gnanamoorthy, G., Algahtani, A., . . . Jeon, B.-H. (2021). A Short Review on the Utilization of Incense Sticks Ash as an Emerging and Overlooked Material for the Synthesis of Zeolites. *Crystals*, *11*(10), 1255. https://doi.org/10.3390/cryst11101255.

Yossadania, A., Hayati, Z., Harapan, H., Saputra, I., Diah, M., & Ramadhana, I. F. (2023). Quantity of antibiotic use and its association with clinical outcomes in COVID-19 patients: A snapshot from a provincial referral hospital in Indonesia. *Narra J*, *3*(3), e272. https://doi.org/10.52225/narra.v3i3.272.

Zainal Abidin, A., Abu Bakar, N. H. H., Ng, E. P., & Tan, W. L. (2017). Rapid Degradation of Methyl Orange by Ag Doped Zeolite X in the Presence of Borohydride. *Journal of Taibah University for Science*, *11*(6), 1070-1079. https://doi.org/10.1016/j.jtusci.2017.06.004.

Zhang, W., Wan, J., Cui, W., Liu, L., Cao, L., Shen, G., & Hu, S. (2019). Adsorption dynamics and mechanism of Amoxicillin and Sulfachlorpyridazine by ZrOx/porous carbon nanocomposites. *Journal of the Taiwan Institute of Chemical Engineers*, *104*, 65-74. https://doi.org/10.1016/j.jtice.2019.08.009.